Estimation of spatial surface energy fluxes and actual evapotranspiration over Ghataprabha river basin using remote sensing data

Shashank C. Bangi[1*] *and Veena S. Soraganvi*[2]

[1]Research Scholar, Department of Civil Engineering, Basaveshwar Engineering College, Bagalkote and Assistant Professor, Department of Civil Engineering, KLS Gogte Institute of Technology, Belagavi, (Karnataka state) India.
[2]Professor, Professor, Department of Civil Engineering, Basaveshwar Engineering College, Bagalkote, (Karnataka state) India

Abstract.: Accurately measuring Actual Evapotranspiration (AET) in spatial scale is a crucial yet challenging task within the hydrological cycle, playing a pivotal role in determining the water requirements of diverse crops. Consequently, precise estimation of Evapotranspiration (ET) at a spatial scale is imperative for regions characterized by arid and semiarid conditions, such as the Ghataprabha river basin. In current study, actual evapotranspiration was estimated using SEBAL algorithm utilizing Landsat-8 satellite data and meteorological data, focusing on the Ghataprabha river basin situated in Karnataka, India. The paper also presents the spatial divergence of Surface Energy Fluxes and Actual Evapotranspiration in correlation with various land use and land cover patterns within the study region. Notably, the ET fraction derived from the SEBAL algorithm demonstrates a commendable correlation with the ET fraction derived from EEFlux (R^2= 0.9). As a result, this study highlights the significance of accurately capturing surface energy fluxes and actual evapotranspiration within heterogeneous field conditions in regional scale.

1 Introduction

Evapotranspiration (ET) is the amalgamation of two processes: evaporation and transpiration. Evaporation pertains to water loss from soil and water surfaces, while transpiration involves water loss from plant structures. Within the hydrological cycle, evapotranspiration holds a prominent role as a significant component. Nonetheless, its accurate measurement remains a challenging endeavour. This phenomenon is predominantly influenced by the equilibrium between water and energy on the Earth's surface and bears substantial relevance to agricultural and irrigation practices.

Various techniques exist for calculating Actual Evapotranspiration (AET), encompassing both direct and indirect approaches, such as empirical, water balance, surface energy balance,

[*] Corresponding author: shashankcbangi@gmail.com

and combined methods. The selection of these methods depends on factors like data accessibility and desired precision. Empirical methods offer promising outcomes primarily in the derived regions. For example, FAO Penman-Monteith method [1], which stands as a prevalent empirical approach for estimating ET within agricultural contexts. In contrast, the water balance method's efficacy hinges on the accurate measurement of other components within the hydrological cycle. Its accuracy is contingent on the precise determination of these variables.

ET exhibits spatiotemporal variability, rendering the requirement for both spatial and temporal ET estimation crucial for effective irrigation planning and scheduling. While ground-based measurement stations accurately capture temporal ET variations, their limitation lies in providing an insufficient spatial distribution due to their point-based nature. Remote Sensing(RS) advancements hold the promise of enabling the estimation of spatial ET across diverse surfaces. Satellite imagery serves as a valuable resource for extracting spatial ET information using the Surface Energy Balance (SEB) approach. The SEB approach operates on the fundamental principle of the conservation of energy. It predominantly focuses on quantifying the residual energy that remains on the surface due to changes in surface conditions. This approach has been elaborated in studies by [2,3].

Numerous algorithms have been used to extract residual energy [4-9]. The SEBI method [4] utilizes a crop water stress index to estimate ET. The SEBS method [7] incorporates roughness height for heat transfer enhancement. The S-SEBI technique [6] offers the potential to estimate ET using only RS data under consistent climatic conditions. METRIC approach [8] provides a solution for estimating ET under high terrain conditions. ReSET [10] employs raster image inputs, enhancing spatial stability. TSEB method discerns separate estimation of evaporation and transpiration. Upon comparing the various energy balance methods, the Surface Energy Balance Algorithm for Land (SEBAL) formulation [5] and its validation [11] exhibit significant potential for successful ET estimation across diverse field conditions [12].

Various researchers have effectively employed the SEB approach to estimate evapotranspiration, yet most of these methods have been limited to agriculturally well-vegetated lands and also there is a deficiency observed for utilization of data in support of ground truth data at regional scale. There exists a scarcity of cases that address semiarid regions, where evapotranspiration holds significant importance within the hydrological cycle. Furthermore, the Ghataprabha river basin faces a pressing need for effective water resource management due to the considerable water demands of the agricultural sector. Consequently, the accurate estimation of AET across the basin scale and the comprehension of its variations over heterogeneous surfaces becomes imperative. The estimation of surface energy components from remotely sensed imagery necessitates high-quality datasets and techniques suited to the specific field conditions. Therefore, this study focus on a methodology that can harness recent advancements in RS technology, including up-to-date satellite imagery and novel RS techniques designed for extracting surface energy fluxes.

In pursuit of this, the study has opted to implement the widely recognized SEBAL method along with ground meteorological data. This choice is driven by the absence of prior research for the Ghataprabha river basin and the well-documented success of SEB methods in semiarid regions. Given that the Ghataprabha river basin is located within such a semiarid region, this approach holds potential for yielding valuable insights.

The study seeks to achieve the following objectives: (1) extract surface energy fluxes, including Net radiation (Rn), Soil heat flux (G), Sensible heat flux (H), and Latent heat flux (LE), from satellite imagery, (2) estimate actual evapotranspiration across the Ghataprabha river basin using the SEBAL algorithm in conjunction with Landsat 8 OLI/TIRS images, (3) assess the effectiveness of the SEBAL algorithm by comparing it with EEflux, and (4)

 https://doi.org/10.1051/e3sconf/202345503008

illustrate the disparities in surface energy fluxes and actual evapotranspiration across diverse Land Use and Land Cover (LULC) categories.

2 Study area and data used

2.1 Study area

The research was conducted within the Ghataprabha river basin, situated between latitudes 15° 45' to 16° 25'N and longitudes 74° 00' to 75° 55' E, depicted in Fig. 1. The Ghataprabha River is positioned in the west side of the Krishna river basin, originating from the Western Ghats of Maharashtra at an elevation of 884m. The river spans approximately 60 Km towards the east, traversing through Sindhudurg and Kolhapur districts of Maharashtra before crossing the Maharashtra-Karnataka border. Within Karnataka, the river flows for 216 Km within the Belagavi district and 283 Km within the Bagalkot district. Its course concludes as it merges with the River Krishna upstream of the Alamatti reservoir. The total catchment area of this sub-basin measures 8829 km^2. The Ghataprabha River commences in the tropical wet climatic zone, progressing through semi-arid and arid zones before joining the River Krishna near the Alamatti reservoir. The annual rainfall is primarily attributed to the south-west monsoon (June-October), contributing around 80% of the total, while the north-east monsoon in winter accounts for the remaining 20%. During summer, temperatures can escalate to 42°C in May and April. Relative humidity fluctuates between 30% and 90% across the non-monsoon and monsoon periods. Rainfall, occurring from June to September, transpires over 12 to 25 days, yielding depths ranging from 175 to 520 mm.

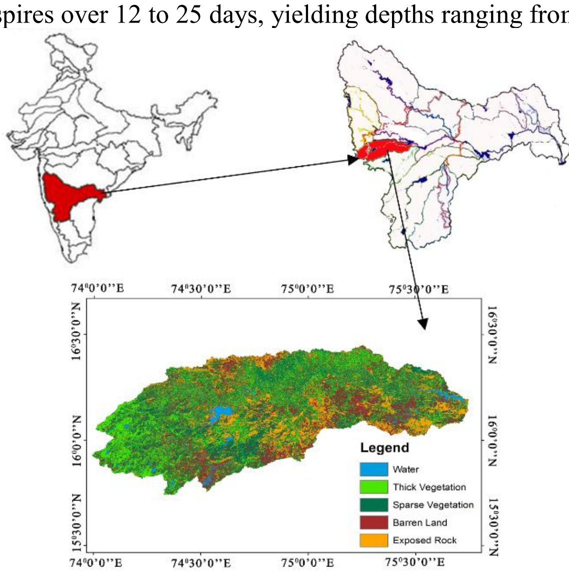

Fig. 1. Study Area (Ghataprabha River basin) with LULC Map

2.2 Data used

The SEBAL algorithm necessitates satellite data capable of providing multispectral observations across the visible, near-infrared, and thermal spectral ranges. For this study, Landsat 8 satellite images from the latest Landsat series were utilized. The satellite possesses 9 spectral bands with spatial resolutions ranging from 15 to 30 meters, capturing information across the visible, near-infrared, and mid-infrared regions. Meanwhile, other 2 thermal bands comprises a spatial resolution of 100 meters, acquiring data from the thermal region [13]. The Ghataprabha river basin falls under the coverage of a single Landsat 8 image located at the 146th path and 49th row. Technical specifications and band details of Landsat 8 OLI/TIRS are shown in Table 1. The data were sourced from Earth Explorer platform by USGS (http://earthexplorer.usgs.gov). Meteorological data were obtained from Automatic Weather Stations (AWS) positioned within the study region, overseen by the Indian Meteorological Department (IMD). A range of meteorological parameters, including temperature, precipitation, wind speed, surface pressure, relative humidity, and solar radiation, were gathered from the website http://dsp.imdpune.gov.in/.

Table 1. Technical specifications of Landsat 8 OLI/TIRS

Sensor type	**OLI, TIRS**
Spatial resolution	30m (100m-thermal, 15m-pan)
Spectral range	0.433-12.5 µm
Number of bands	11
Temporal resolution	16 days
Image size	183 X 170 km
Swath	183 km

3 Methodology

For this investigation, the SEBAL algorithm is embraced to compute actual evapotranspiration. The step-by-step process for estimating AET through the SEBAL approach is illustrated in a sequential flowchart, as depicted in Fig. 2. The calculation of the Earth's surface reflectance involves quantifying the proportion of incident energy that is reflected. Distinct features on the Earth's surface have varying energy reflection patterns, allowing for the differentiation and identification of these features through their reflectance characteristics. The downloaded data are typically presented in the form of Digital Numbers (DN), necessitating the conversion of these digital values into reflectance values. The rescaling coefficient, supplied within the metadata, serves as a conversion factor that transforms DN into Top of the Atmosphere (TOA) reflectance. Surface albedo is determined as the ratio of the reflected energy to the incident energy. It can be characterized as the surface's capability to reflect incoming energy, thereby illustrating its reflective attributes [14]. The Normalized Difference Vegetation Index (NDVI) is a commonly employed metric that assesses the vitality and density of vegetation based on sensor data. It is computed from spectral measurements obtained at two distinct bands: the red and near-infrared wavelengths [15]. Surface emissivity is the proportion of thermal energy emitted from a surface relative to the thermal energy emitted from a blackbody at the identical temperature. Land Surface Temperature (LST) represents the radiative temperature emitted from the Earth's surface, and its derivation from Thermal Infrared Sensor (TIRS) data involves a three-step process. Initially, digital numbers extracted from the TIRS image were transformed into top-of-atmosphere radiance using predefined calibrated values specific to the sensor. Subsequently, these radiance values were further converted into brightness temperature. In the final step, temperature correction was executed, incorporating the emissivity factor [16].

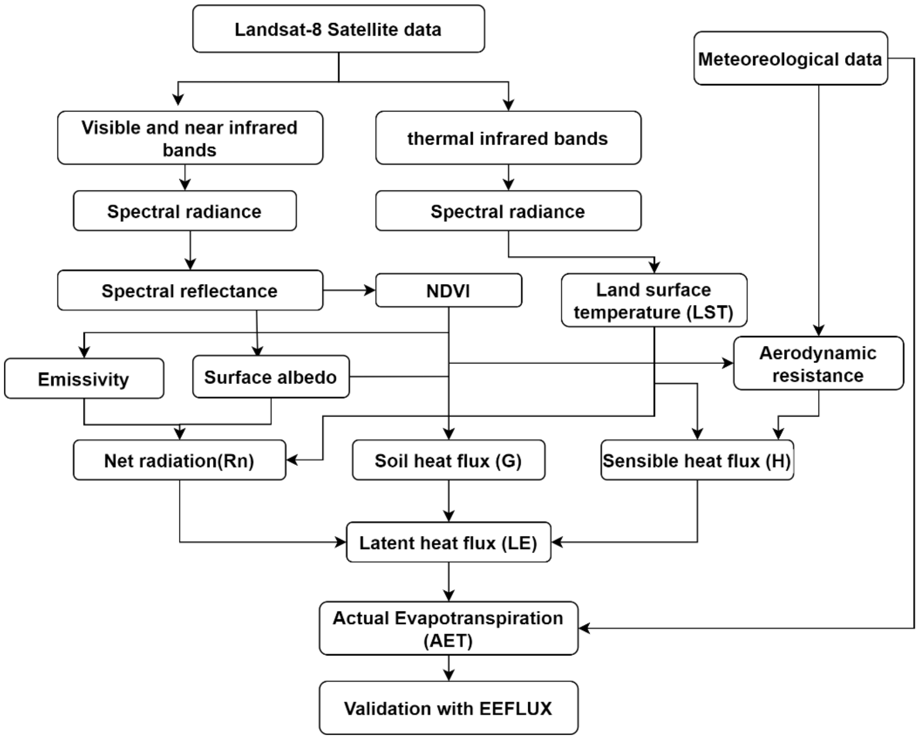

Fig. 2. Methodology chart

Net radiation corresponds to the residual energy retained within the surface, computed as the cumulative sum of incoming and outgoing short and long wave energy [17]. Soil heat flux denotes the pace at which heat is absorbed and held within the soil and vegetation owing to the presence of moisture. Sensible heat flux represents the speed at which heat is released from the surface to the air via processes of convection and conduction, primarily driven by temperature disparities between the surface and the surrounding air. The Latent Energy flux (LE) was determined as the remaining energy on the surface, calculated through the utilization of other surface energy fluxes, as depicted in equation (14). This value signifies the energy accessible on the surface for the evaporation of water. Instantaneous LE was transformed into instantaneous evapotranspiration (ET) by utilizing the latent heat of vaporization, which represents the amount of heat absorbed when a kilogram of water undergoes evaporation. The reference evapotranspiration (ET) fraction was obtained by calculating the ratio of the computed instantaneous ET for each pixel to the reference ET computed from weather data. Ultimately, daily evapotranspiration (ET) was derived from ET_{rf} by relating it to the 24-hour reference ET, as illustrated in equation (1).

$$ET_{24} = ET_{rf} \ X \ ET_{r\_24} \quad (1)$$

Here, ET_{24} signifies the 24-hour evapotranspiration, and ET_{r_24} represents the 24-hour reference evapotranspiration computed from meteorological data.

4 Results and discussion

Surface albedo (α) portrays the capacity of the land surface to reflect solar energy it receives. Generally, objects with lighter colors reflect more energy, whereas those with darker colors reflect less energy. Consequently, objects with lighter shades exhibit higher surface albedo in comparison to darker counterparts [18]. For the study conducted on February 9th, 2014, spatially distributed surface albedo was computed across the study area, as depicted in Fig. 3. It was noted that the Ghartaprabha river basin exhibited α values ranging from 0.01, the lowest, to 0.40, the highest. Notably, the lowest surface albedo was primarily observed over waterlogged and wet surfaces, a result of water's substantial energy absorption capabilities. This property makes wet surfaces easily distinguishable through their surface albedo. Conversely, dry rocky terrain and developed areas showcased the highest surface albedo due to their light color and heightened reflectivity. α values associated with vegetation demonstrated variations lying between those of waterlogged areas and dry rocky surfaces.

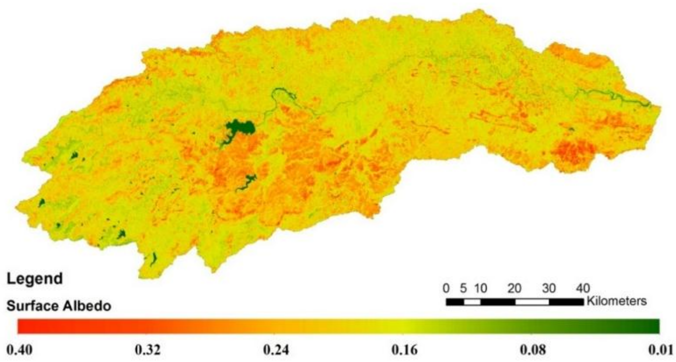

Fig. 3. Spatial distribution of Surface Albedo

The spatial variation of NDVI across the study area was generated, as displayed in Fig. 4. Land surfaces characterized by extensive vegetation cover and elevated chlorophyll content typically exhibit heightened vegetation indices. Thus, the trees thriving in the western hill region showcased notably elevated NDVI values, which gradually declined towards the northern and southern regions from the river due to the limited water availability for crop growth. Conversely, water surfaces, dry rocky terrains, and barren lands registered lower NDVI values due to the non-appearance of vegetation. The recorded NDVI spanned from a highest value of 0.54 to a lowest of -0.25. Notably, features that exhibit greater reflection in the red wavelength than in the near-infrared wavelength result in negative NDVI values [19].

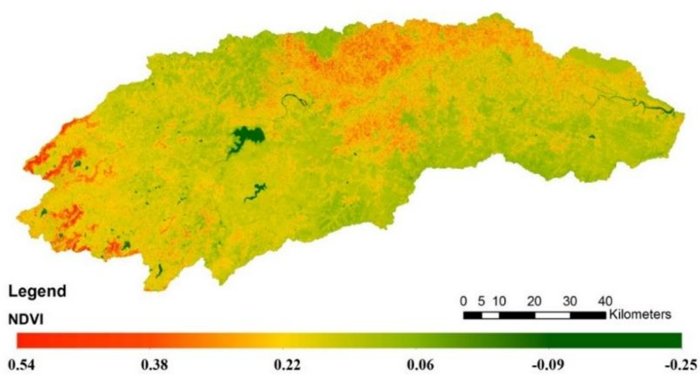

Fig. 4. Spatial distribution of NDVI

LST was derived using Band 10 of Landsat 8, as illustrated in Fig. 5. Across the study area, surface temperatures ranged from 295 K to 318 K. Lower temperatures were evident over water surfaces, while higher temperature was observed over dry terrain. Temperature fluctuations on vegetation surfaces were influenced by water availability [20], resulting in a temperature increase from the river towards the northern and southern portions of the study area. Notably, areas featuring water and vegetation near the river and the western side (encompassed by the Western Ghats) exhibited lower temperatures. The spatial variation in LST provided by satellite-derived data enabled the easy identification and differentiation of dry and wet surfaces [21]. Wet soil exhibited lower temperatures in comparison to dry soil due to the existence of water.

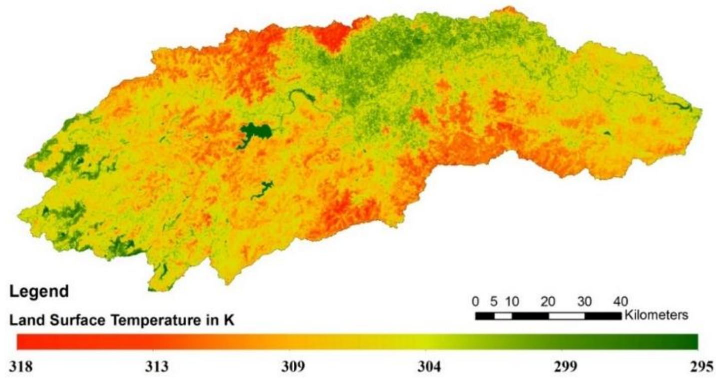

Fig. 5. Spatial distribution of LST

Fig. 6 illustrates the Net Radiation values acquired on February 9th, 2014. The range of Net Radiation observed spanned from a maximum of 486 W/m² to a minimum of 53 W/m². The Net Radiation primarily hinges on the radiation received by the surface and radiation reflected from it. Surfaces that reflect more radiation, such as dry rocky terrain and built-up areas, exhibited lower net radiation due to the limited energy availability at the surface. Conversely, water surfaces, which reflect less radiation, demonstrated higher net radiation. Notably, the net radiation values decreased towards the northern and southern sectors of the area due to water scarcity and heightened reflectivity. Vegetation with high water content and elevated NDVI values displayed increased net radiation when compared to vegetation with lower water content and diminished NDVI.

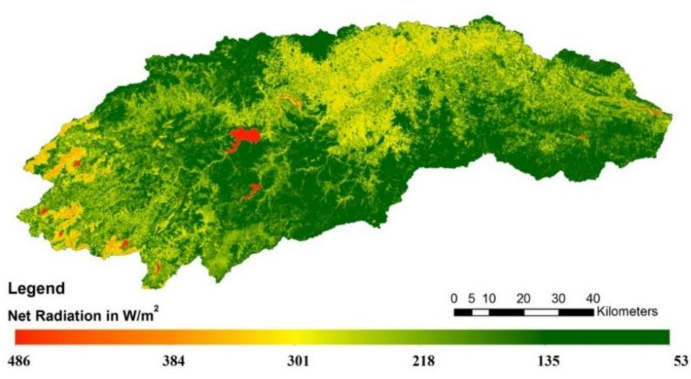

Fig. 6. Spatial distribution of Net radiation

Soil heat flux (G) primarily relies on the soil's capacity to absorb heat. This heat absorption capability increases with greater soil water content, as water reflects less energy and absorbs more. Notably, the wet surfaces within the study area exhibited elevated soil heat flux values compared to the drier surfaces. The northern and southern sections predominantly consist of dry rocky terrain, resulting in lower G values in those regions (Fig.7). Areas beside the river are primarily dedicated to agriculture and benefit from ample water through irrigation, leading to higher observed soil heat flux values. The western part of the study area receives substantial rainfall, further contributing to elevated soil heat flux values.

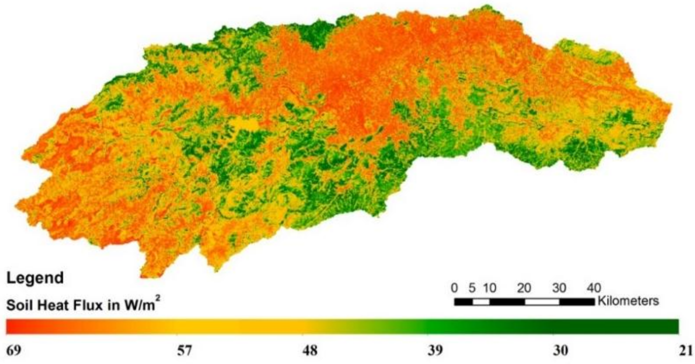

Fig. 7. Spatial distribution of soil heat flux

The disparity between surface temperature and air temperature holds great importance in the determination of sensible heat flux (H). Consequently, sensible heat flux tends to be higher in regions where the temperature difference between the surface and the air is pronounced. Surfaces with lower temperatures, such as water bodies and dense vegetation, exhibit reduced sensible heat flux due to the diminished temperature contrast between the surface and the air. Conversely, areas with high temperature differences, like dry rocky terrain and barren land, experience heightened sensible heat flux as the air is cooler compared to the hot, dry surface. Across the study area, the maximum recorded sensible heat flux reached 146 W/m², while the minimum registered value was 0 W/m², as illustrated in Fig. 8.

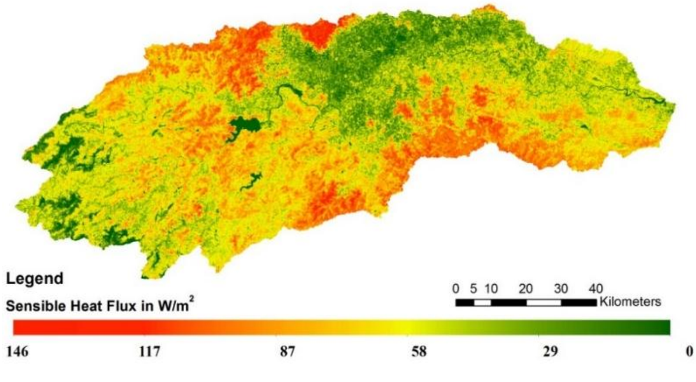

Fig. 8. Spatial distribution of sensible heat flux

Latent heat flux (LE) pertains to the energy expended in the process of water evaporation from a surface. This flux is chiefly reliant on the energy that remains at the surface following its utilization by soil heat flux and sensible heat flux. Within the study area, water surfaces showcased the highest latent heat flux values, primarily attributed to water's diminished reflectivity and heightened energy absorption capacity. Fig.9 visually emphasizes that a significant portion of the incoming energy directed at water surfaces is devoted to water evaporation. Following water surfaces, wet and vegetated areas demonstrated elevated latent heat flux values due to the combined effects of transpiration from vegetation and soil evaporation. Conversely, dry lands and rocky surfaces displayed minimal latent heat flux due to the absence of water. Within this region, latent heat flux values decreased moving from the river towards the northern and southern regions. The western region, characterized by substantial rainfall and lush vegetation, exhibited a noteworthy increase in latent heat flux values.

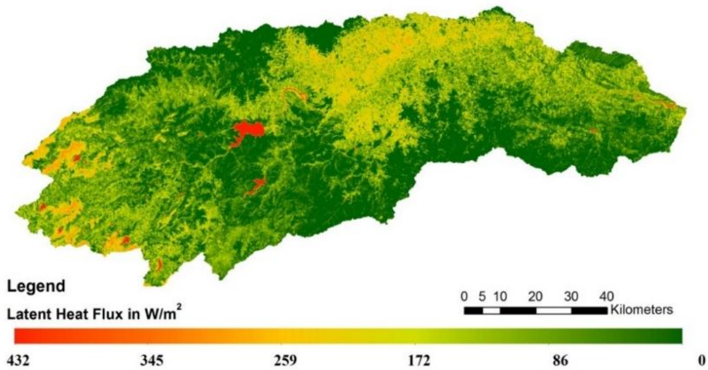

Fig. 9. Spatial distribution of Latent heat flux

The Actual Evapotranspiration values for February 9th, 2014, are illustrated in Fig. 10. Within the study area, the range of observed values spanned from a maximum of 3.72 mm/day to a minimum of 0 mm/day. The magnitude of actual evapotranspiration primarily hinges on the availability of water and energy at the surface [22]. Consequently, water surfaces exhibited higher evapotranspiration values compared to other features within the area. Evapotranspiration values displayed an increasing trend moving towards the river from the northern and southern edges of the study area. Additionally, elevated evapotranspiration values were recorded in the western part of the study area, attributable to abundant vegetation cover and higher rainfall. Conversely, surfaces characterized by dry rocky terrain and barren land exhibited negligible evapotranspiration, nearly approaching 0 mm/day.

The Evaporative fraction obtained from EEFlux (Earth Engine Evapotranspiration Flux) (https://eeflux-level1.appspot.com) was utilized as a reference to validate the ET produced by the SEBAL algorithm. EEFlux, which operates on the Google Earth Engine system, is grounded in the METRIC algorithm. EEFlux data, available since 1984, spans the entire globe and is tied to Landsat data. To calibrate the SEB for the image, EEFlux employs NLDAS gridded weather data in the US and CFSV2 gridded weather data globally. The Evaporative fraction derived via the SEBAL algorithm was correlated with the evaporative fraction from EEFlux. This correlation demonstrated a notable level of agreement, with a correlation coefficient (R^2) of 0.9, as depicted in Fig. 11. EEFlux has emerged as a valuable platform for validating regional-scale evapotranspiration across diverse and heterogeneous surfaces, addressing the scarcity of available regional-scale ET data.

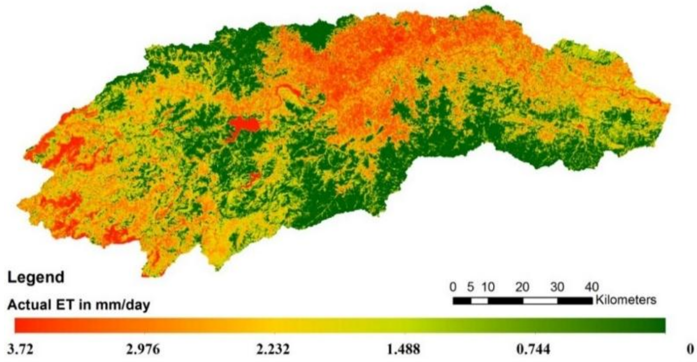

Fig. 10. Spatial distribution of actual evapotranspiration

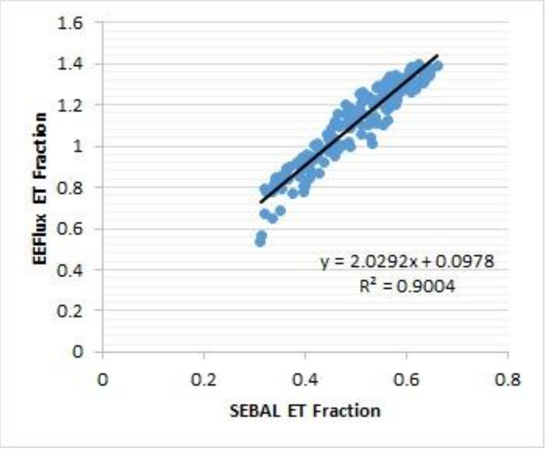

Fig. 11. Correlation between the derived ET fraction from SEBAL and ET fraction from EEflux

5 Conclusion

In this current study, the estimation of AET was carried out for the Ghataprabha river basin on February 9th, 2014. The process involved the utilization of Landsat 8 OLI/TIRS satellite imagery in conjunction with meteorological data to extract Surface Energy fluxes and Actual Evapotranspiration. With a spatial resolution of 30 meters, this study achieved fine-grained results, enabled by the enhanced 16-bit radiometric resolution of Landsat 8 satellite images. As a result, this study underscores the significance of extracting surface energy fluxes and actual evapotranspiration within diverse field conditions. The findings highlight substantial spatial variation in actual evapotranspiration across the study area. The spatial distribution of actual evapotranspiration maps reveals a gradual decrease in values moving from the river to the catchment's ridge, extending towards the northern and southern parts of the catchment. Consequently, it can be deduced that the majority of agricultural fields in the study region rely on river water for irrigation purposes. Ground surface parameters, encompassing vegetation types, LST, and surface albedo, exert a noteworthy influence on the spatial distribution of surface energy fluxes and actual evapotranspiration. Hence, a sensitivity analysis involving different parameters can streamline the evapotranspiration estimation process, representing a potential avenue for future work. The successful application of Landsat 8 OLI/TIRS data for estimating Actual Evapotranspiration within the Ghataprabha river basin on a regional scale is well demonstrated by this study. The outcomes hold practical utility for online irrigation management, contributing not only to water conservation but also enhancing crop productivity. However, it's important to note that this study is applicable solely to cloudless satellite images, and due to the limited temporal resolution of Landsat 8 OLI/TIRS data, obtaining daily actual evapotranspiration values throughout the entire year is not feasible.

References

1. A. G. Richard, P. Luis, Raes, Dirk and S. Martin. FAO Irrigation and Drainage Paper Crop. Irrigation and Drainage **(56):** 300 (1998).
2. Sogaard, Henrik, and H. Segaard. Estimation of the Surface Energy Balance in the Sahelian Zone of Western Africa, Geografisk Tidsskrift-Danish Journal of Geography, **88:1**, 108-115, (2013).
3. Anapalli, S. Saseendran, R.Timothy, K.N. Reddy, H. Prasanna. Gowda, S. Ruixiu, D. K. Fisher, J. Moorhead, and G. Marek. Application of an Energy Balance Method for Estimating Evapotranspiration in Cropping Systems. Agricultural Water Management, **204**, 107–17. (2018)
4. M. Menenti and B. J. Choudhury, Parameterization of Land Surface Evaporation by Means of Location Dependent Potential Evaporation and Surface Temperature Range. Proceedings of IAHS Conference on Land Surface Processes **212**, 561–68. (1993)
5. Bastiaanssen, G. M. Bastiaanssen, H. Pelgrum, J. Wang, Y. Ma, J.F. Moreno, G. J. Roerink and T. Van Der Wal. A Remote Sensing Surface Energy Balance Algorithm for Land (SEBAL) Formulation. Journal of Hydrology **(1–4)**, 213–29. (1998)
6. Roerink, G. Z. Su, and M. Menenti. S-SEBI: A Simple Remote Sensing Algorithm to Estimate the Surface Energy Balance. Physics and Chemistry of the Earth, Part B: Hydrology, Oceans and Atmosphere **25 (2),** 147–57. (2000).
7. Z. Su. The Surface Energy Balance System (SEBS) for Estimation of Turbulent Heat Fluxes. Hydrology and Earth System Sciences **6**, 85–100. (2002).
8. A. G. Richard, M. Tasumi, A. Morse, R. Trezza, L. James. Wright, W. Bastiaanssen, W. Kramber, I. Lorite, and W. Robison. Satellite-Based Energy Balance for Mapping Evapotranspiration with Internalized Calibration (METRIC)—Applications. Journal of Irrigation and Drainage Engineering **133 (4),** 395–406. (2007).
9. M. Castelli, M. C. Anderson, Y. Yang, G. Wohlfahrt, G. Bertoldi, G. Niedrist, A. Hammerle, P. Zhao, M. Zebisch, and C. Notarnicola. Two-Source Energy Balance Modeling of Evapotranspiration in Alpine Grasslands. Remote Sensing of Environment **209**, 327–42. (2018).
10. E. Aymn. ReSET-Raster: Surface Energy Balance Model for Calculating Evapotranspiration Using a Raster Approach. Journal of Irrigation and Drainage Engineering. **137(4),** 203–10. (2011).
11. W. G. Bastiaanssen, G.M. Bastiaanssen, H. Pelgrum, J. Wang, Y. Ma, J.F. F. Moreno, G. J. J. Roerink, and T. Van Der Wal. A Remote Sensing Surface Energy Balance Algorithm for Land (SEBAL) Validation. Journal of Hydrology, **212–213** 213–229. (1998).
12. L. A. Yuei and S. Kumar. Evapotranspiration Estimation with Remote Sensing and Various Surface Energy Balance Algorithms-a Review. Energies **7 (5)**, 2821–49. (2014).

13. U.S. Geological Survey (USGS). Landsat 8 Fact Sheet. Fact Sheet 2013-3060, **3–6**. (2013).
14. Tasumi, Masahiro, R. G. Allen, and R. Trezza. At-Surface Reflectance and Albedo from Satellite for Operational Calculation of Land Surface Energy Balance. Journal of Hydrologic Engineering, **13**, 51–63. (2008).
15. Guha, Subhanil, H. Govil, A. Dey, and N. Gill. Analytical Study of Land Surface Temperature with NDVI and NDBI Using Landsat 8 OLI and TIRS Data in Florence and Naples City , Italy. European Journal of Remote Sensing **51(1)**, 667–78. (2018)
16. Y. Xiaolei, X. Guo, and Z. Wu. Land Surface Temperature Retrieval from Landsat 8 TIRS-Comparison between Radiative Transfer Equation-Based Method, Split Window Algorithm and Single Channel Method. Remote Sensing. ***6*(10),** 9829-9852. (2014).
17. Z. A. Samani, D. V. Tran, M. Bleiweiss, and R. Skaggs. Estimating Daily and 24-Hour Net Radiation for All Sky Conditions through Remote Sensing and Climatic Data. Journal of Irrigation and Drainage Engineering, **139**, 3. (2013).
18. Burakowski, Elizabeth, A.Tawfik, A. Ouimette, L. Lepine, K. Novick, S. Ollinger, C. Zarzycki, and G. Bonan. The Role of Surface Roughness, Albedo, and Bowen Ratio on Ecosystem Energy Balance in the Eastern United States, Agricultural and Forest Meteorology. **249**, 367-376. (2018).
19. P. M. Seevers and R. W. Ottmann. Evapotranspiration Estimation Using a Normalized Difference Vegetation Index Transformation of Satellite Data. Hydrological Sciences Journal **39 (4),** 333–45. (1994)
20. Ning, Jicai, Z. Gao, R. Meng, F. Xu, and M. Gao. Analysis of Relationships between Land Surface Temperature and Land Use Changes in the Yellow River Delta. Frontiers of Earth Science **12 (2),** 444–56. (2018).
21. Zeng, Fanxing and N. Gao. Use of an Energy Balance Model for Studying Urban Surface Temperature at Microscale. Procedia Engineering **205**, 2956–2966. (2017).
22. Sun, Zhongping, B. Wei, W. Su, W. Shen, C. Wang, D. You, and Z. Liu. Evapotranspiration Estimation Based on the SEBAL Model in the Nansi Lake Wetland of China. Mathematical and Computer Modelling **54 (3–4):** 1086–92. (2011).